Geophysical Research Letters

Supporting Information for

Can coastal upwelling trigger a climate mode? A study on intraseasonal-scale coastal upwelling off Java and the Indian Ocean Dipole

Takanori Horii[1], Eko Siswanto[2], Iskhaq Iskandar[3], Iwao Ueki[1], and Kentaro Ando[1]

1. Global Ocean Observation Research Center, Research Institute for Global Change, Japan Agency for Marine-Earth Science and Technology, 2-15, Natsushima, Yokosuka, Kanagawa 237-0061 Japan

2. Earth Surface System Research Center, Research Institute for Global Change, Japan Agency for Marine-Earth Science and Technology, 3173-25, Showa-machi, Kanazawa, Yokohama, Kanagawa 236-0001, Japan

3. Faculty of Mathematics and Natural Sciences, Sriwijaya University, Jl. Masjid Al Gazali, Bukit Lama, Palembang 30128, Indonesia

Contents of this file

Introduction

This Supporting Information contains text, a table, and figures that provide additional information to support the descriptions and analyses in the article.

Satellite-based Chl-a data contain missing values, and the error estimate is essential in creating a proxy for the coastal upwelling along the southern coast of Java. Text S1 describes a method for estimating the error range of the average Chl-a.

Text S2 describes the procedure for decomposing the surface temperature advection (Section 4) into climatological and anomalous components.

Table S1 and Figures S1–4 are supplementary materials cited in the main text and this Supporting Information.

Text S1.

In order to quantify the influence of missing values in calculating the average Chl-a (Figure S1), a proxy of the coastal upwelling along the southern coast of Java, we conducted a statistical experiment using processed Chl-a data (1/8°×1/8°) in 2019 (a pIOD year). In 2019, many observations were obtained without missing values. In the experiment, we prepared multiple Chl-a distributions by superimposing missing-value distributions on the actual snapshots that originally did not contain a missing value in the target area. Then, we evaluated multiple data to estimate the error range of area-averaged Chl-a as follows.

In 2019, the number of days when we were able to observe the area south of Java without a missing value was 160 days. For the period from April to October 2019, the average observation rate was 99.3%.

First, we prepared 492, 605, and 909 snapshots, the data acquisition rates of which were 75%, 50%, and 25%, respectively, based on the actual Chl-a snapshots during 2003–2020 (Figure S2a). For example, for the 605 examples in which both the observed and missing values are 50%, we adopted snapshots with 40% to 60% observed values. Then, we randomly increased or decreased the boundary between the observed and missing values (in other words, increased or decreased the clouds) to adjust the rate to 50%. We did the same for the cases of 75% and 25%.

Second, we used the processed multiple snapshots as a spatial filter with the distribution of 1/NaN, where "1" and "NaN" denote observations and missing values, respectively. We randomly selected the multiple 1/NaN distributions and applied them to the 2019 Chl-a observation data south of Java, and prepared a 365-day timeseries. This procedure was repeated 1,000 times. Thus, we artificially prepared "cloudy" conditions and tested how many observations would be needed to reproduce the Chl-a-based proxy of the coastal upwelling signals.

Using the 1,000 timeseries, we estimated the error range of average Chl-a, which depends on the observation rate and average Chl-a amplitude. Figure S2b shows an example of the one standard deviation based on the 1,000 Chl-a timeseries assuming the observation rates of 50%. We estimated the relationship (ratio) between the original Chl-a amplitude and the standard deviation from the 1,000 timeseries by least-squares fitting, based only on the 160 days without a missing value. The standard deviation increased linearly as the observation rate decreased from 75%, 50%, to 25% (figure not shown). We estimated the error range according to the actual observation rate (0% to 100%) from this relationship. Finally, the error range of average Chl-a timeseries south of Java during 2003–2020 was estimated from the average Chl-a amplitudes and the observation rates for the region south of Java.

We also conducted a second experiment in which we randomly prepared 75%, 50%, and 25% snapshots from the Chl-a data during 2003–2020, reflecting only the probability distribution of the observations. However, this must not be natural because synoptic-scale clouds south of Java are distributed on a spatial scale of several hundred kilometers (Fig. S2a). The results of the second experiment were not conservative. Therefore, in the present study, the results in the first experiment were considered as error ranges in the Chl-a timeseries.

The error range at the first Chl-a blooming in each year is shown in Figure S3. In the error range shown here, the observation error of satellite-observed Chl-a data (0.12 mg/m^3; Xu et al., 2021) was also added.

Text S2.

In order to calculate the horizontal advection of ocean mixed-layer temperature for the diagnosis of temperature balance in the southeastern Indian Ocean (Section 4), we used two satellite-based datasets. Sea surface temperature (SST) data were provided from the National Oceanic and Atmospheric Administration (NOAA) daily optimum interpolation (OI) SST dataset on a 0.25°×0.25° grid (Reynolds et al. 2007). Ocean surface current data were the Ocean Surface Current Analysis-Real Time (OSCAR) data on a 1/3°×1/3 grid (Bonjean and Largerloef, 2002). Since there were several missing values in the coastal area before 2003, we focused on the period of 2003–2020. We re-gridded the SST data onto an OSCAR grid, and horizontal temperature advection was calculated using current velocity and temperature gradient (central differences). This assumes that the SST gradient and OSCAR velocities are representatives of the horizontal gradient and velocity of the ocean mixed layer, respectively. The validity of the calculation was evaluated in our previous studies (Horii et al. 2013).

We calculated the advection terms as daily time steps. The OSCAR data were interpolated from the original data in steps of five to six days to obtain daily values by the spline method.

The climatologies (mean seasonal cycle) and anomalies of SST, surface current, and horizontal temperature advection were calculated using the following procedures. First, based on the 2003–2020 timeseries, the annual cycle and the first three harmonics were estimated by least-squares fitting and were used as the mean seasonal cycle (climatologies). Anomalies are defined as the deviation from the mean seasonal variation.

In order to understand how anomalous temperature advections occurred with the coastal upwelling south of Java, the surface currents and horizontal temperature gradients were decomposed to the following expressions:

$$U = \langle U \rangle + U', \quad V = \langle V \rangle + V', \quad T = \langle T \rangle + T',$$

where the angled brackets denote the mean seasonal cycle (climatology) and the prime denotes the anomalies. The zonal and meridional advections can be decomposed as

$$U T_x = \langle U \rangle \langle T_x \rangle + \langle U \rangle T_x' + U' \langle T_x \rangle + U' T_x' \quad (1)$$

$$V T_y = \langle V \rangle \langle T_y \rangle + \langle V \rangle T_y' + V' \langle T_y \rangle + V' T_y' \quad (2).$$

In the right-hand sides of equations (1) and (2), the terms $\langle U \rangle \langle T_x \rangle$ and $\langle V \rangle \langle T_y \rangle$ represent the climatological temperature advections and the other terms are the anomalies. The terms $U' T_x'$ and $V' T_y'$ are the nonlinear advection terms described in Section 4 (Figure S4).

Table S1. List of year, IOD condition during July–October, date of first Chl-a blooming, and data availability during April–September. The IOD condition was defined as ±0.5 of the average Dipole Mode Index (DMI). The date shows the first significant Chl-a signal exceeding 0.45 (two standard deviations of Chl-a variability from April to June).

Year	IOD	Date: The first Chl-a blooming	Available Chl-a data (April–September)
2003	pIOD	June 8, 2003	95.1 %
2004	Neutral	June 13, 2004	91.2 %
2005	nIOD	July 19, 2005	91.2 %
2006	pIOD	June 7, 2006	93.7 %
2007	pIOD	June 8, 2007	94.7 %
2008	pIOD	May 22, 2008	91.9 %
2009	Neutral	June 29, 2009	91.3 %
2010	nIOD	June 27, 2010	75.6 %
2011	pIOD	June 3, 2011	86.5 %
2012	pIOD	May 24, 2012	97.0 %
2013	Neutral	July 15, 2013	85.9 %
2014	Neutral	August 11, 2014	87.4 %
2015	pIOD	May 14, 2015	92.4 %
2016	nIOD	N/A	86.7 %
2017	pIOD	May 11, 2017	93.2 %
2018	pIOD	May 13, 2018	97.8 %
2019	pIOD	April 24, 2019	99.7 %
2020	Neutral	June 20, 2020	95.5 %

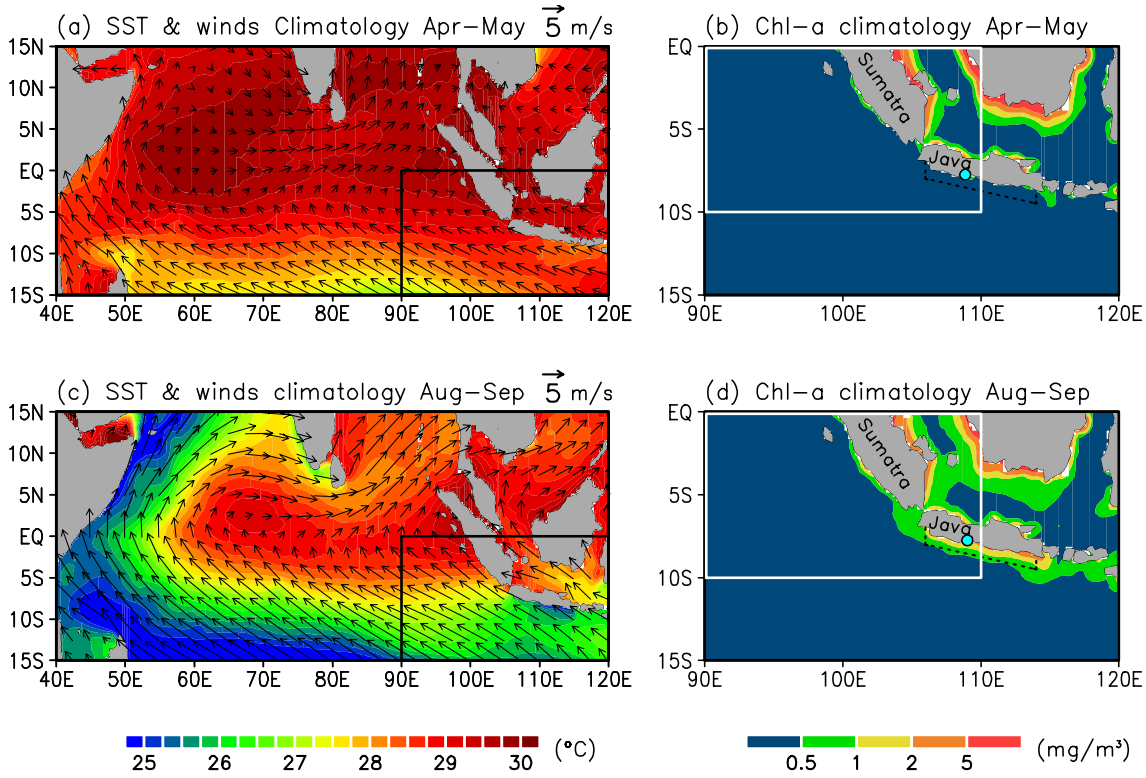

Figure S1. (a) Climatological mean SST and surface winds in April–May. (b) As in (a), but the surface Chl-a concentration for the region 90°E–120°E, 15°S–0° (inset in Figure 1a). The white square represents the eastern pole (90°E–110°E, 10°S–0°) for the calculation of the Dipole Mode Index (DMI) (Saji et al., 1999). The region enclosed by the black dashed lines south of Java (6.5°S, 106°E)–(9.0°S, 114°E) shows the area for the average of Chl-a concentration. A light-blue circle at 7.8°S, 109°E indicates the location of Indonesian tidal station. (c) and (d) As in (a) and (b), respectively, but in August–September.

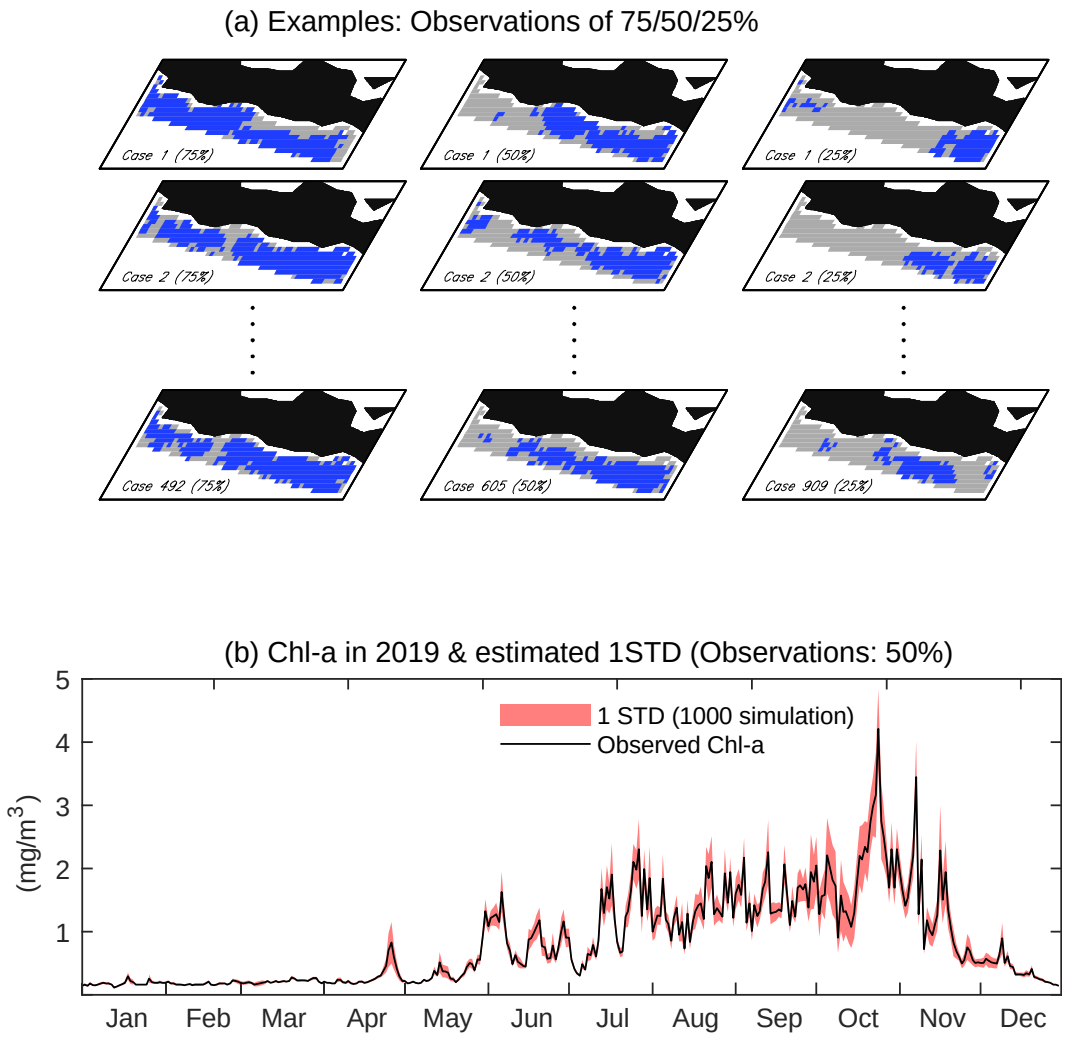

Figure S2. (a) Examples of snapshots with observed and missing values. Blue (gray) grids denote observed (missing) data. Left, middle, and right columns show observed (missing) data of 75% (25%), 50% (50%), and 25% (75%), respectively. The numbers of snapshots during 2003–2020 are 492, 605, and 909, respectively. (b) Timeseries of chlorophyll-a (Chl-a) concentration (mg/m^3) averaged for the region south of Java (see Figure S1 for the map). The light red shading indicates one standard deviation based on simulated 1,000 timeseries using spatial filters in which both the observed and missing values are 50% (see Text S1 for the details).

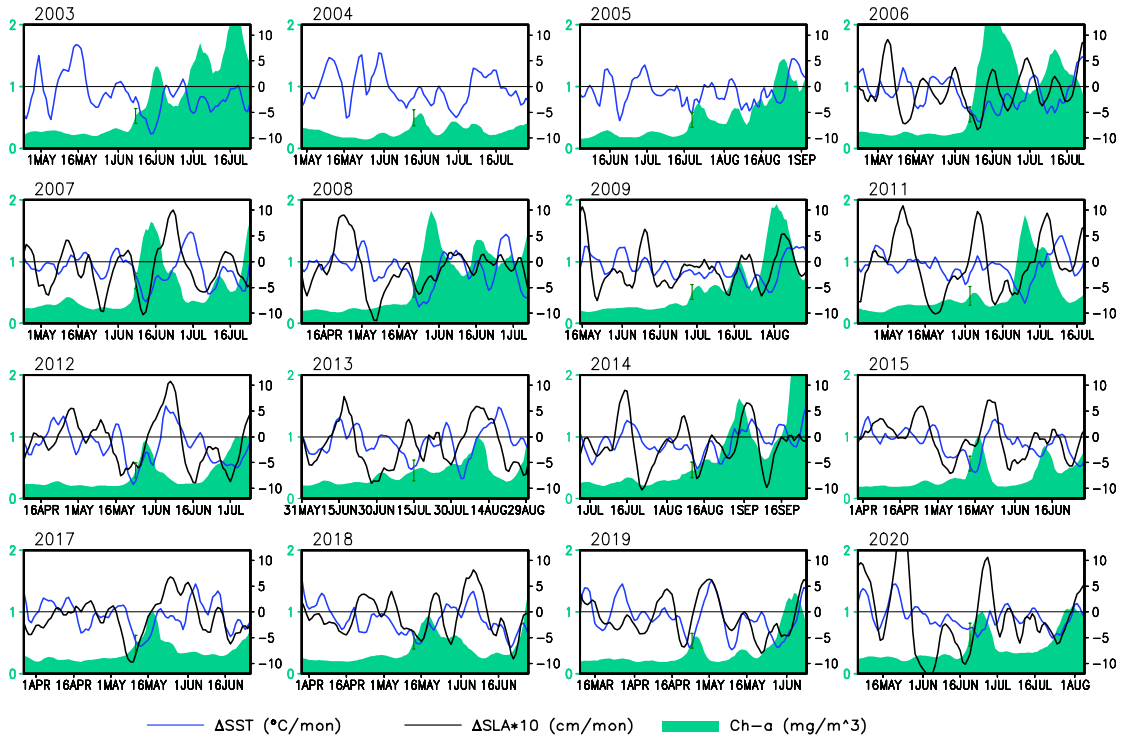

Figure S3. Timeseries of Chl-a concentration south of Java (green shading; mg/m^3; left axis), temporal changes of SSTA (blue; °C/month; right axis) and SLA (black; ×10 cm/month; right axis). The SSTA was averaged for the same region as the Ch-a. A five-day running mean filter was applied to the data. The timeseries show from day −30 to day +30 centered on the first Chl-a blooming of each year. Data for 2010 and 2016 are omitted due to the small amplitudes of Chl-a.

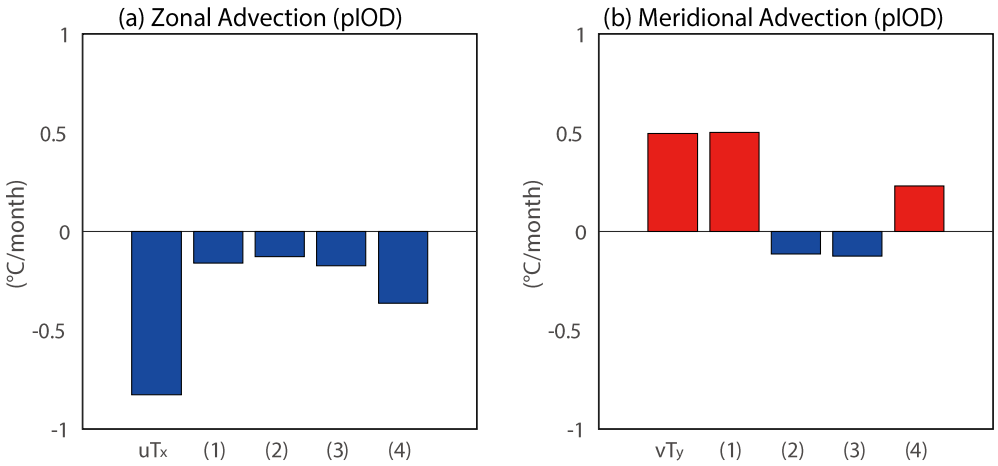

Figure S4. Composite surface temperature advection terms for (a) zonal and (b) meridional components from day 0 to day +30 based on the first coastal upwelling signals for 10 pIOD years. The temperature advection ($u\,T_x$) is decomposed to the climatologies and anomalies as (1) $\langle u \rangle \langle T_x \rangle$, (2) $\langle u \rangle\, T_x'$, (3) $u' \langle T_x \rangle$, and (4) $u'\, T_x'$, respectively, where u (T_x) denotes the zonal surface current (temperature gradient), brackets denote the climatologies, and primes indicate anomalies. The meridional components ($v\,T_y$) are shown in the same way. Positive (negative) values indicate warming (cooling) of the area (100°E–110°E, 10°S–5°S) described in Section 4 and Figure 4.